Soft Matter

Theory for the Casimir Effect and the Partitioning of Active Matter

Journal:	*Soft Matter*
Manuscript ID	SM-ART-10-2020-001797.R1
Article Type:	Paper
Date Submitted by the Author:	10-Nov-2020
Complete List of Authors:	Kjeldbjerg, Camilla M.; California Institute of Technology, Division of Chemistry and Chemical Engineering Brady, John F.; California Institute of Technology, Division of Chemistry and Chemical Engineering

Soft Matter

ARTICLE TYPE

Cite this: DOI: 00.0000/xxxxxxxxxx

Theory for the Casimir Effect and the Partitioning of Active Matter

Camilla M. Kjeldbjerg and John F. Brady*

Received Date
Accepted Date

DOI: 00.0000/xxxxxxxxxx

Active Brownian Particles (ABPs) distribute non-homogeneously near surfaces, and understanding how this depends on system properties—size, shape, activity level, etc.—is essential for predicting and exploiting the behavior of active matter systems. Active particles accumulate at no-flux surfaces owing to their persistent swimming, which depends on their intrinsic swim speed and reorientation time, and are subject to confinement effects when their run or persistence length is comparable to the characteristic size of the confining geometry. It has been observed in simulations that two parallel plates experience a "Casimir effect" and attract each other when placed in a dilute bath of ABPs. In this work, we provide a theoretical model based on the Smoluchowski equation and a macroscopic mechanical momentum balance to analytically predict this attractive force. We extend this method to describe the concentration partitioning of active particles between a confining channel and a reservoir, showing that the ratio of the concentration in the channel to that in the bulk increases as either run length increases or channel height decreases. The theoretical results agree well with Brownian dynamics simulations and finite element calculations.

1 Introduction

Many natural systems can be described as active matter: the flocking of birds, humans walking in crowded areas, the movement of bacteria, Janus particles in suspension, etc[1–3]. Active matter systems consist of "particles" that convert chemical energy into mechanical energy leading to self-propulsion[4]. These movements generate internal stresses and can drive systems far from thermodynamic equilibrium[5]. Active matter systems exhibit interesting phenomena such as particle accumulation near surfaces and self-assembly due to their persistent motion. For instance, Janus particles can accumulate at the corners of a micro-gear causing it to rotate and generate mechanical work[6–8].

Active Brownian Particles (ABPs) are a model active matter system: ABPs move with a swim speed U_0 in a direction $\boldsymbol{q}$ for a characteristic reorientation time τ_R; the average length they move between reorientations is called the run, or persistence, length $\ell = U_0\tau_R$[9]. This model is illustrated in Fig. 1. Some of the interesting properties of active particles are due to the fact that they often have an effective size—their run length—which can be much larger than their geometric size such that they experience confinement in geometries whose size is on the order of the run length[10–14]. Galajda et al.[15] showed that placing *E. coli* in a square container divided by Chevron-shaped barriers (shown in Fig. 1(b)) would concentrate the bacteria on one side of the container. This behavior is profoundly different from purely passive Brownian particles, which would homogeneously fill a volume independent of the geometric shape. The partitioning of *E. coli* is a direct result of the bacteria having a persistent motion with a run length much larger than both their size and the size of the funnel-shaped openings. Di Giacomo et al.[16] have utilized this persistent motion to sequester motile bacteria by deploying 3-dimensional micro-traps.

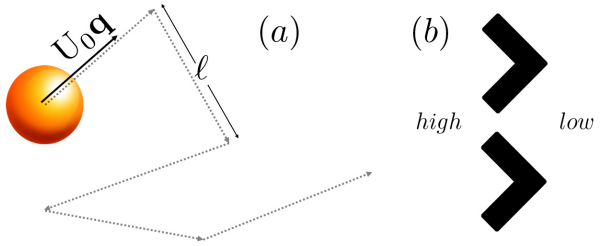

Fig. 1 (a) Example of an ABP's random movement with swim speed U_0 in a direction $\boldsymbol{q}$, reorientation time τ_R and run length $\ell = U_0\tau_R$. (b) Chevron-shaped barriers (from[15]).

Our aim in this work is to describe how active particles partition in simple geometries such as a channel of size H when placed in contact with an infinite reservoir of ABPs as depicted in Fig. 5. What is the ratio of the average concentration in the channel to that in the infinite reservoir? Active systems are inherently far from equilibrium, and we cannot appeal to equilibrium thermodynamic properties such as the chemical potential to predict the

Division of Chemistry and Chemical Engineering, California Institute of Technology, Pasadena, CA 91125 USA. E-mail: jfbrady@caltech.edu

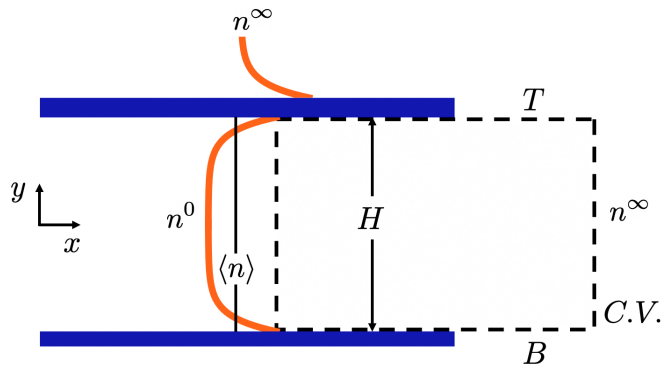

Fig. 2 Illustration of two parallel plates in an active bath. The plates are separated by a distance H. C.V. denotes the control volume for the mechanical balance.

partitioning. Fortunately, active particles are still subject to the laws of mechanics, and we show that a simple macroscopic balance allows one to predict behavior without detailed calculations.

To illustrate our approach, we first consider the attraction between two parallel plates (also called the Casimir effect[17]) and show that the average concentration between the plates equals that in the bulk reservoir independent of the degree of confinement. This leads to a simple analytical expression for the attractive force. We then study the partitioning in the previously mentioned channel geometry of Fig. 5 and show that the behavior is fundamentally different, with the average concentration growing linearly with the ratio of the run length to the channel spacing. The analysis is then extended to a periodic array of plates in contact with an infinite reservoir where we show how the parallel plates results transition to those of the channel when the thickness of the plates exceeds 6 times the run length.

2 Attraction between parallel plates: The Casimir effect

One of the simplest examples of confinement is two parallel plates separated by a gap distance H immersed in an infinite bath of particles as shown in Fig. 2. For passive systems the parallel plates will experience an attractive force towards each other when the gap spacing is on the order of the particle diameter, $H \sim 2a$. This attraction is often referred to result from the disjoining pressure[18,19] or the Casimir effect in quantum mechanics[20,21], and in colloid science it is known as depletion flocculation[22]. For active systems, Yan & Brady[13] and Ray et al.[17] showed, in independent studies, that for infinitely long walls the pressure on the interior walls depends on the gap spacing, and as the gap spacing decreases the pressure decreases as well. Additionally, Ray et al.'s simulation study showed that there is an attraction between parallel plates immersed in a bath of active particles.

The attraction arises from the difference in the forces exerted by the active particles on the interior and exterior plate surfaces. We quantify this force difference with, $\Delta\Pi/\Pi^{\mathrm{W}}_{out}$, where $\Delta\Pi = \Pi^{\mathrm{W}}_{out} - \Pi^{\mathrm{W}}_{in}$, and Π^W is the force/unit area, or pressure, exerted by the ABPs on the plate surfaces.

An inherent property of active matter is that the particles accumulate at walls (and more generally at no-flux surfaces) due to their persistent motion. Yan & Brady[13] showed that the pressure on a single isolated wall is given by

$$\Pi^W_{out} = n^\infty(k_BT + k_sT_s), \tag{1}$$

where n^∞ is the number density far from the wall, k_BT is the thermal energy, and $k_sT_s = \zeta U_0\ell/2$ is the active energy, which is a measure of the activity level of the ABPs. Here, ζ is the Stokes drag coefficient of an ABP, and we are considering two-dimensional reorientation processes giving rise to the factor 2 in (1).

As shown by Yan & Brady[13] the expression for the pressure on the inner wall for two infinitely long plates is the same as (1), but with the centerline concentration n^0 replacing n^∞. Thus, the net attractive force is given by the simple relation

$$\frac{\Delta\Pi}{\Pi^{\mathrm{W}}_{out}} = 1 - \frac{n^0}{n^\infty}. \tag{2}$$

The above expression holds when the accumulation boundary layers at each wall do not overlap, which is true for moderate to high activity ($k_sT_s/k_BT > 50$) and when the run length is comparable to the gap spacing. To complete the description, however, we need a relation between n^0 and n^∞; that is, we need to know how the APBs partition between the parallel plates and the surrounding reservoir.

For a thermodynamic system, such as charged plates in an ionic solution, the partitioning is determined by equating the chemical potentials inside and outside, $\mu_{in} = \mu_{out}$. The electrostatic system shares similarities with the active system: ions accumulate (or deplete) near the charged plates and display a non-homogeneous distribution between the plates[23]. However, since the ionic system is at equilibrium the flux of each ion is zero at each and every point between the plates and in the reservoir. Thus, the centerline concentration of each ion is related to the reservoir concentration via its chemical potential: $n_i^0 = n_i^\infty \exp\left(-z_i e\phi^0/k_BT\right)$, where n_i^∞ is the reservoir concentration of ion i, z_i is its valency, e is the elementary charge, and ϕ^0 is the potential at the centerline (relative to a zero level in the reservoir), which depends on the surface charge density on the plates. The attraction between the plates is then determined by a force balance and can be shown to be given by the ion osmotic pressure difference between the inside and the outside.

Active particles systems are inherently out of equilibrium and we cannot appeal to the chemical potential nor to a point-wise vanishing flux. For a dilute suspension of APBs, the particle distribution is governed by the Smoluchowski equation for the probability density $P(\boldsymbol{x}, \boldsymbol{q}, t)$ for finding a particle at position $\boldsymbol{x}$ with orientation $\boldsymbol{q}$ at time t:

$$\frac{\partial P(\boldsymbol{x}, \boldsymbol{q}, t)}{\partial t} + \nabla \cdot \boldsymbol{j}^T + \nabla_R \cdot \boldsymbol{j}^R = 0, \tag{3}$$

where the translational and rotational fluxes are $\boldsymbol{j}^T = U_0\boldsymbol{q}P -$

$D_T\nabla P$ and $\boldsymbol{j}^R = -D_R\nabla_R P$, respectively. Here, D_T and D_R are the translational and rotational diffusivities; the reorientation time $\tau_R = 1/D_R$. The orientational gradient operator is $\nabla_R = \boldsymbol{q}\times\nabla\boldsymbol{q}$.

To make progress and capture the essential features of the distribution of ABPs, we expand the Smoluchowski equation in the first few orientational moments: the zeroeth moment is the concentration $n(\boldsymbol{x},t) = \int P(\boldsymbol{x},\boldsymbol{q},t)d\boldsymbol{q}$, the first moment is the polar order $\boldsymbol{m}(\boldsymbol{x},t) = \int \boldsymbol{q}P(\boldsymbol{x},\boldsymbol{q},t)d\boldsymbol{q}$, etc. For 2D, the orientational moments satisfy a hierarchy of equations[24]:

$$\frac{\partial n}{\partial t} + \nabla\cdot\boldsymbol{j}_n = 0, \tag{4}$$

$$\frac{\partial \boldsymbol{m}}{\partial t} + \nabla\cdot\boldsymbol{j}_m + D_R\boldsymbol{m} = 0, \tag{5}$$

where the fluxes are

$$\boldsymbol{j}_n = U_0\boldsymbol{m} - D_T\nabla n, \tag{6}$$

$$\boldsymbol{j}_m = U_0\boldsymbol{Q} + \frac{1}{2}U_0 n\boldsymbol{I} - D_T\nabla m. \tag{7}$$

Here, n is the number density, $\boldsymbol{m}$ is the polar order and $\boldsymbol{Q}$ is the nematic order, $\boldsymbol{Q}(\boldsymbol{x},t) = \int(\boldsymbol{qq} - \frac{1}{2}\boldsymbol{I})P(\boldsymbol{x},\boldsymbol{q},t)d\boldsymbol{q}$, with $\boldsymbol{I}$ the isotropic tensor. The boundary conditions we impose are a constant number density in the reservoir far from the plates n^∞, and no polar or nematic order, $\boldsymbol{m}^\infty = 0$, $\boldsymbol{Q}^\infty = 0$, etc. The plates are hard no-flux walls, such that $\boldsymbol{n}\cdot\boldsymbol{j}^T = 0$ on the plates, where $\boldsymbol{n}$ is the surface normal, and the angular reorientation is unaffected by the plates.

While the system's behavior is fully determined from the Smoluchowski equation (3), its solution, or that of the moment equations (4)-(5), for any but the simplest geometries is a daunting task. Dimensional analysis shows that the distribution of particles between the plates depends on four lengths: the length of the plates L, the plates' separation H, the run length $\ell = U_0\tau_R$, and the microscopic diffusive step length $\delta = \sqrt{D_T\tau_R}$. The ratio of the run length ℓ to the microscopic length δ is also a measure of the active energy compared to the thermal energy $k_sT_s/k_BT = (\ell/\delta)^2/2$.

We are interested in large plates where $L \gg H$ and $L \gg \ell$, and high activity $\ell/\delta \gg 1$. In this limit the force or pressure on the plates scales as the active pressure $n^\infty(k_BT + k_sT_s)$ and depends only on the confinement ℓ/H. Furthermore, to determine the attractive force between the plates we only need an estimate of the centerline concentration—the partitioning between the reservoir and the plates. To accomplish this, we can appeal to a mechanical momentum balance.

At the microscopic level the particles evolve according to the over-damped Langevin equation[24]:

$$0 = -\zeta\boldsymbol{U}_\alpha + \zeta U_0\boldsymbol{q}_\alpha + \boldsymbol{F}^B_\alpha\,, \tag{8}$$

where ζ is the Stokes drag coefficient, $\boldsymbol{U}_\alpha$ is the velocity of particle α, and $\boldsymbol{q}_\alpha$ is its orientation. Each particle is also subject to random thermal forces $\boldsymbol{F}^B_\alpha$ that give rise to translational Brownian motion, and which are characterized by $\overline{\boldsymbol{F}^B} = 0$ and $\overline{\boldsymbol{F}^B(0)\boldsymbol{F}^B(t)} = 2k_BT\zeta\delta(t)\boldsymbol{I}$, where the overline denotes averaging over the thermal fluctuations of magnitude k_BT and $\delta(t)$ is the Dirac delta function. The orientation vector $\boldsymbol{q}_\alpha$ undergoes a random reorientation process giving rise to rotary Brownian motion as detailed in appendix A. (The Smoluchowski equation (3) is the Fokker-Planck equation corresponding to the microscopic dynamics (8).)

From the microscopic dynamics (8) we can write a corresponding linear momentum or force balance[24]:

$$0 = -\zeta\boldsymbol{j}_n + \zeta U_0\boldsymbol{m} + \nabla\cdot\boldsymbol{\sigma}^{osmo}\,, \tag{9}$$

where the flux is given by $\boldsymbol{j}_n \equiv n\frac{1}{N}\sum_{\alpha=1}^N\boldsymbol{U}_\alpha$, the polar order is $\boldsymbol{m} \equiv n\frac{1}{N}\sum_{\alpha=1}^N\boldsymbol{q}_\alpha$, and $\boldsymbol{\sigma}^{osmo} = -nk_BT\boldsymbol{I}$ is the osmotic pressure. In the force balance (9) $-\zeta\boldsymbol{j}_n$ is the average drag force from the suspending medium (which is assumed to be stationary), $\zeta U_0\boldsymbol{m}$ is the average propulsive or swim force, and since the average of the Brownian force is zero, its effect appears as the divergence of a stress $\nabla\cdot\boldsymbol{\sigma}^{osmo}$.

The similarity between the momentum balance (9) and the number density flux (6) is no coincidence—the flux is the mobility, $1/\zeta$, times the driving force, and the driving forces are the average swim force, $\zeta U_0\boldsymbol{m}$, and the stress gradient from Brownian motion, $\nabla\cdot\boldsymbol{\sigma}^{osmo}$. (The Stokes-Einstein-Sutherland relation connects the translational diffusivity to the drag, $D_T = k_BT/\zeta$.)

We now apply this momentum balance to the control volume (C.V.) illustrated in Fig. 2. Integrating the x-component over the C.V. gives

$$\langle n\rangle k_BT - n^\infty k_BT = \frac{1}{H}\int_{C.V.}(\zeta U_0 m_x - \zeta j_x^n)\,dxdy\,, \tag{10}$$

where $\langle n\rangle = \frac{1}{H}\int ndy$ is the average concentration between the plates as illustrated in Fig. 2. Equation (10) is just a statement that the net body force in the C.V. is balanced by the osmotic pressure difference.

From (5) at steady state the polar is $\boldsymbol{m} = -\tau_R\nabla\cdot\boldsymbol{j}_m$ and thus with (7) for the flux (10) becomes

$$\begin{aligned}(\langle n\rangle - n^\infty)(k_BT + k_sT_s) = {}& -2k_sT_s\langle Q_{xx}\rangle \\ & + \frac{2}{H}\int_T\left(k_sT_sQ_{xy} - D_T\frac{\partial m_x}{\partial y}\right)dx \\ & - \frac{1}{H}\int_{C.V.}\zeta j_x^n dxdy\,,\end{aligned} \tag{11}$$

where the activity $k_sT_s = \zeta U_0^2\tau_R/2$ and the integral in the second line is over the 'top' T in Fig. 2. Along the plate $\boldsymbol{n}\cdot\boldsymbol{j}_m = 0$ and the integral over B is the same as over T; hence, the factor of 2. In obtaining (11) we have used the fact that far from the exit of the plates, both between the plates and into the reservoir, there is no variation with respect to x. We note that the balance is now with the active pressure—the sum of the osmotic pressure and the swim pressure[24,25].

The first term on the RHS of (11) is the average nematic order at the left boundary of the C.V. far from the ends of the plates. Because $\boldsymbol{Q}$ is traceless, $\langle Q_{xx}\rangle = -\langle Q_{zz}\rangle$, and we can estimate

$\langle Q_{xx}\rangle$ from the infinite parallel plate solution of Yan & Brady[13], which shows that this term is negligible ($|\langle Q_{xx}\rangle| < 0.005\langle n\rangle$ for $\ell/\delta = 45$ and $\ell/H \in [0,3]$).

The integrals on the RHS of (11) are only nonzero at the edges of the plates. In the reservoir j_x^n is zero, as it is between the plates far from the edge. Fig. 10 shows that the magnitude of $\partial m_x/\partial y$ is small and localized in a very small region right at the exit of the plates. Thus, the mechanical balance predicts that $\langle n\rangle \approx n^\infty$. This balance has a very simple physical interpretation: the force per unit area of the left boundary of the C.V., which is the active pressure between the plates times the height $\langle n\rangle(k_BT + k_sT_s)H$, is equal to the force per unit area on the right boundary of the C.V., which the active pressure in the reservoir times the height $n^\infty(k_BT + k_sT_s)H$.

The value of $\langle n\rangle/n^\infty$ measured from Brownian Dynamics simulation is shown in the inset of Fig. 3 as a function of confinement ℓ/H with a plate length of $L/\ell = 10$; as expected the connection is exact for passive particles $\ell/H \to 0$ and saturates to a constant as ℓ/H increases. For large ℓ/H the average concentration between the plates is roughly 20% higher than the concentration in the bulk, which we believe to be caused by the finite thickness of the plates (in simulation) that adds an additional surface where particles accumulate and generate polar order which effects the macroscopic mechanical momentum balance. This is confirmed in § 4 on periodic plates, where partitioning is determined as a function plate thickness, d, and reaches equal partitioning when $d/\ell \to 0$.

Finally, we need to relate the centerline concentration n^0 to $\langle n\rangle$. For this we use the exact solution for the distribution between two parallel walls (assumes isotropic nematic order, which is a good approximation for simple systems) of Yan & Brady[13]:

$$\frac{n(y)}{n^0} = 1 + \frac{1}{2}\left(\frac{\ell}{\delta}\right)^2 \frac{\sinh(\lambda y) + \sinh(\lambda(H-y)}{\sinh(\lambda H)}, \qquad (12)$$

where λ is the inverse thickness of the accumulation boundary layer, or the inverse screening length, $\lambda = \sqrt{1+(\ell/\delta)^2/2}/\delta$. A straightforward integration over y relates n^0 to $\langle n\rangle$. In the limit of high activity $\lambda H \gg 1$, which is the most interesting case, we have

$$\frac{n^0}{\langle n\rangle} = 1 - \frac{1}{1+(H/\ell)/\sqrt{2}}. \qquad (13)$$

Fig. 3 shows a comparison between the predicted centerline concentration, using the mechanical balance's estimate of $\langle n\rangle \approx n^\infty$, and results from Brownian dynamics (BD) simulations. (See appendix A for a description of the BD simulations.) The simulations are for a highly active system with strong confinement such that the smallest length H, is on the order of the run length, and the degree of confinement ℓ/H, is varied by changing the distance between the plates. Edge effects are minimized, since the parallel plates are made much longer than the particles' run length and the channel height. (The data in Figs. 3 and 4 are for $L/\ell = 10$ and $k_sT_s/k_BT = 1012.5$.) There is good qualitative agreement between the predicted center concentration from (13) and the one observed in the BD simulations.

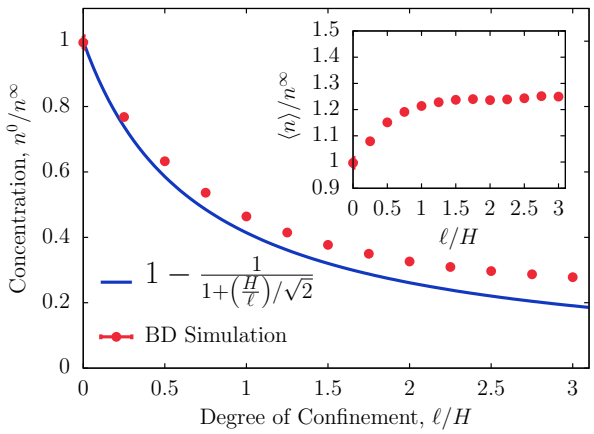

Fig. 3 Centerline concentration, n^0/n^∞, as a function of the confinement, ℓ/H, for parallel walls. The relation $1 - 1/(1 + (H/\ell)/\sqrt{2})$ is derived from a simple mechanical balance. The inset shows the average concentration as a function of the degree of confinement.

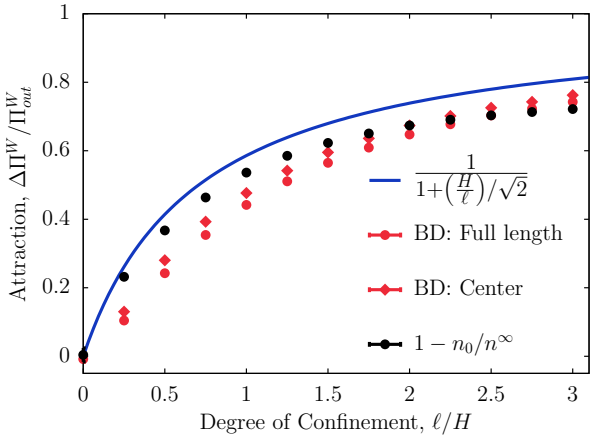

Fig. 4 Attraction between parallel plates, $\Delta\Pi^W/\Pi^W_{out}$, as a function of the degree of confinement, ℓ/H. The relation $1/(1 + (H/\ell)/\sqrt{2})$ is the predicted attraction from a simple mechanical balance, and $1-n^0/n^\infty$ is based on measuring concentration at the centerline via BD simulations.

From (2) the predicted attractive force is

$$\frac{\Delta\Pi}{\Pi^{\mathrm{W}}_{out}} = \frac{1}{1+(H/\ell)/\sqrt{2}}, \qquad (14)$$

which is compared to BD simulations in Fig. 4. In the BD simulations when a particle colloids with a wall it exerts a force on the wall and the pressure is then the sum of individual particle contributions. In the simulations we used a potential-free algorithm[26–28] to model a hard-particle force (see appendix A). The prediction gives a good estimate for the attraction, both for that measured for the full length and the one measured only on the central portion ($1/3L$) of the plates. As expected, the edge effects decrease the attractive force.

It should be appreciated that (14) is an a priori prediction with no adjustable parameters. All we needed to know was the behavior for two infinite parallel walls and then the macroscopic

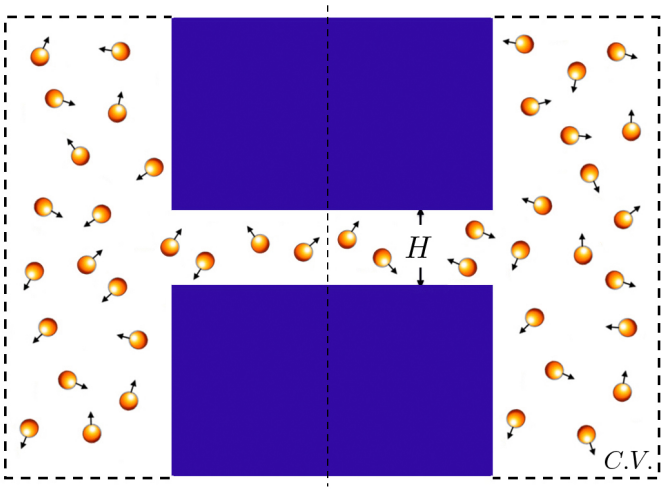

Fig. 5 Illustration of two reservoirs connected by a channel of height H. The concentration of ABPs in the reservoir far from the channel is n^∞.

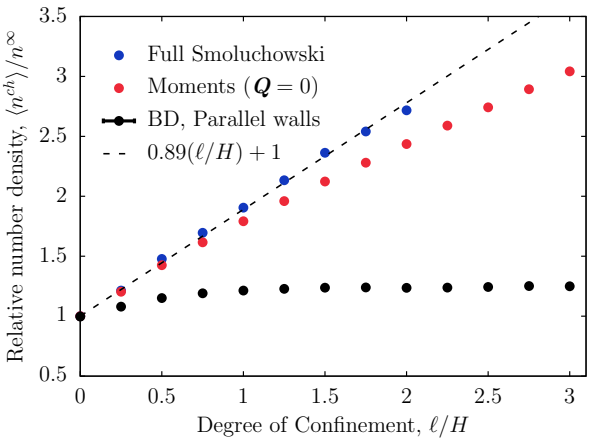

Fig. 6 Numerical solution for the relative number density in a channel, $\langle n^{ch}\rangle/n^\infty$, as a function of degree of confinement, ℓ/H. The Brownian dynamics solution to the parallel plates geometry discussed earlier is also shown for comparison.

momentum balance for the partitioning into the parallel plates.

In the next section, we provide an example of a similar geometry that nevertheless exhibits a completely different behavior, but one that can also be predicted through an analogous macroscopic momentum balance.

3 Channel Confinement

We now investigate the effect of confinement on ABPs in a channel of height H connected to a reservoir as shown in Fig. 5. This geometry is interesting because for passive Brownian particles the partitioning between parallel plates and a channel is the same. This is also true for an ionic solution—the ion concentration in the channel or parallel plates is the same given by the equality of chemical potentials. As we shall see, for active particles the situation is profoundly different.

In Fig. 6 we show the average concentration in the channel far from the ends, $\langle n^{ch}\rangle/n^\infty$, as a function of confinement ℓ/H, along with the data for the parallel plates. The parallel plate results are for BD simulations with $\ell/\delta = 45$ and $L/\ell = 10$. For the channel geometry we solved the full Smoluchowski equation (3) numerically using a standard Galerkin P2-FEM method with adaptive mesh refinement. The finite element method was carried out in *Freefem++*[29]. We also solved numerically the moment equations (4)-(7) (with the $\boldsymbol{Q}=0$ closure) with *Freefem++*. The dashed line in the figure is from BD simulations which have been fit to the linear relation: $\langle n^{ch}\rangle/n^\infty = 1 + 0.89(\ell/H)$. Rather than saturate to a value of approximately unity as for the parallel plates, in the channel geometry the average concentration grows linearly with the degree of confinement! How can we explain this startling difference?

An explanation is provided by considering the behavior of the APBs at the channel opening and combining this with the mechanical momentum balance over a properly chosen control volume. In Fig. 7(a) ABPs slide along the solid wall resulting in a uniform concentration along the wall of magnitude $n^W = n^\infty(1+(\ell/\delta)^2/2) = n^\infty(1+k_sT_s/k_BT)$, where n^∞ is the concentration far from the wall[13]. In Fig. 7(b) as particles slide along the wall from above and below the opening, they escape into the channel rather than continuing along the wall. This results in a deficit of particles just below and above the wall facing into the reservoir. This deficit is quantified in Fig. 8, and we see that it extends over a length $\Delta \approx 3\ell$ independent of both the degree of confinement, ℓ/H, and the level of activity, $k_sT_s/k_BT = (\ell/\delta)^2/2$.

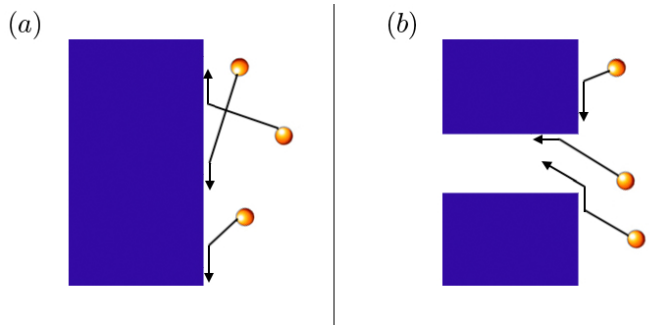

Fig. 7 Illustration of (a) a wall with particles colliding and then sliding along the it and (b) a wall with an opening where they also slide along it but then move into the channel.

As before, we integrate the x-momentum balance (9) over a C.V. that is the dashed lines in Fig. 1 making use of (7) as before:

$$(\langle n^{ch}\rangle - n^\infty)(k_BT + k_sT_s) = -2k_sT_s\langle Q_{xx}\rangle - \frac{1}{H}\int_{C.V.}\zeta j_x^n dxdy - \frac{2}{H}\int_0^\Delta(\Pi^W - \Pi^\infty)dy\,, \qquad (15)$$

where $\langle n^{ch}\rangle = \frac{1}{H}\int n(y)dy$, Π^W is the particle pressure on the wall facing the reservoir, and $\Pi^\infty = n^\infty(k_BT + k_sT_s)$ is the active

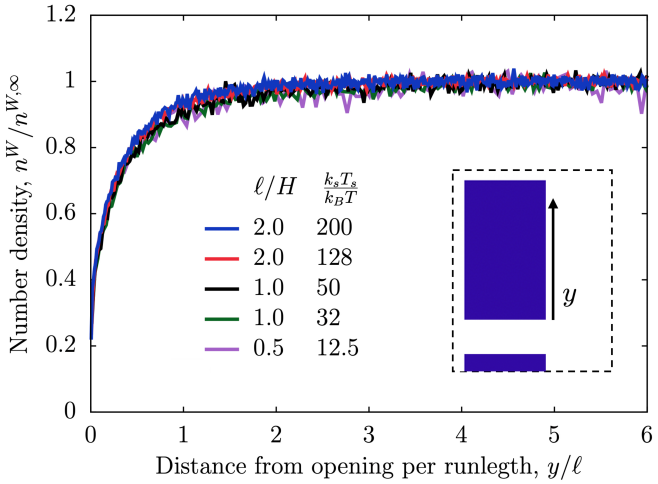

Fig. 8 Number density at the wall normalized by the number density at the wall far from the opening as a function of distance from channel opening per run length measured from BD simulations. All the curves collapse onto one another independently of both degree of confinement and activity.

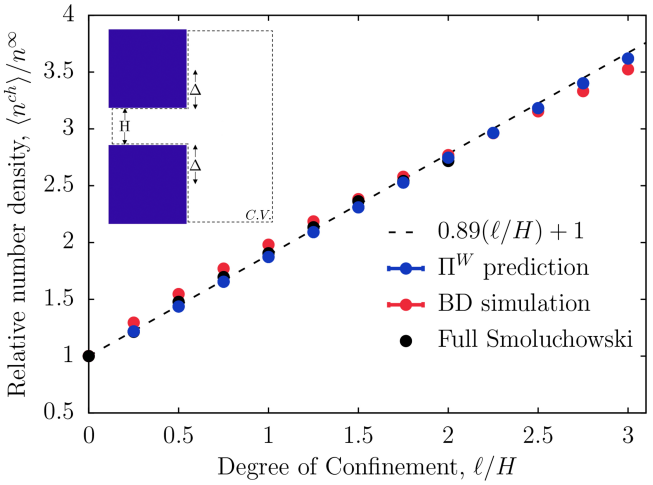

Fig. 9 Relative number density in channel, $\langle n^{ch}\rangle/n^\infty$, as a function of the degree of confinement, ℓ/H. The inset shows the control area for the force balance. Δ is the length of the region at the wall experiencing a decreased pressure due to ABPs escaping into the channel.

pressure in the reservoir. The integral is over the concentration deficit at the wall. As for the parallel plates, the contributions from $\langle Q_{xx}\rangle$ and the integral of the flux are small. The result then has again a very simple physical interpretation: the total pressure on the left boundary of the C.V., $\langle n^{ch}\rangle(k_BT+k_sT_s)H + 2\int_0^\Delta \Pi^W dy$, is equal to that on the right boundary, $n^\infty(k_BT + k_sT_s)(H+2\Delta)$. Thus, the final expression for the partitioning is

$$\frac{\langle n^{ch}\rangle}{n^\infty} = 1 + \left(\frac{2}{H}\right)\frac{\int_0^\Delta[\Pi^\infty - \Pi^W(y)]dy}{\Pi^\infty}, \qquad (16)$$

where $\Pi^W(y) = n^W(y)k_BT$ is the pressure on the wall at a distance y from the opening. Since the deficit is independent of confinement, ℓ/H, and activity, k_sT_s/k_BT, as shown in Fig. 8, we can compute the integral in (16) for one condition and use it to predict the partitioning for all conditions. We used the Π^W determined from BD simulations for $\ell/H = 2$ and $k_sT_s/k_BT = 10^3$. Fig. 9 shows excellent agreement between the predicted channel concentration from the macroscopic momentum balance and that from BD simulations and the solution of the full Smoluchowski equation.

Selection of the proper control volume is important in obtaining an accurate estimate of the partitioning. For example, for the channel geometry one could use a C.V. that is the same as for the parallel plates. If this C.V. were used, then instead of the integral over the pressure deficit along the wall facing the reservoir, one would have instead the integral along the 'top' as in (11): $+\frac{2}{H}\int_T\left(k_sT_sQ_{xy} - D_T\frac{\partial m_x}{\partial y}\right)dx$. (There is no integral on the top boundary in (15) because far from the channel exit we have the behavior of a single isolated wall in contact with the reservoir.) Fig. 10 shows that the $\partial m_x/\partial y$ is much larger and longer ranged for the channel geometry than the parallel plates, and thus, while this term's contribution is small for the parallel plates, it is not for the channel. The important point is that the C.V used in each geometry led to the very simple physical balance between the pressures on the two surfaces and thus to a reasonable estimate for the partitioning.

4 Periodic plates

As a last example we consider the periodic plate geometry illustrated in the inset of Fig. 11. This geometry is intermediate between the parallel plates in an active bath and the channel connected to a reservoir. As the thickness of the plates, d, becomes very thin one expects the partitioning to behave like the parallel plates shown earlier, but without the Casimir attraction since the plates are now placed periodically. In the other limit when the plate thickness becomes very large we expect the behavior to resemble the single channel geometry. Fig. 11 shows the relative number density between the periodic plates compared to that in the reservoir for BD simulations with $k_sT_s/k_BT = 1012.5$ and $L/\ell = 10$. We recover the two limiting behaviors: as $d/\ell \to 0$, $\langle n\rangle/n^\infty \to 1$, and for large d/ℓ the partitioning grows with ℓ/H.

The similarity of the curves in Fig. 11 suggest that they can be collapsed onto a single curve. We define a scaled concentration profile by first subtracting off the parallel plates result and then normalizing by the channel result for $d/\ell \gg 1$:

$$\frac{\overline{\Delta\langle n\rangle}}{n^\infty} = \frac{\langle n\rangle/n^\infty - 1}{\lim\limits_{d/\ell\to\infty}\left(\frac{\langle n\rangle}{n^\infty} - 1\right)}. \qquad (17)$$

This collapse is shown in Fig. 12. Furthermore, the macroscopic momentum balance that led to (16) can be applied here by simply replacing Δ with $d/2$. Thus, from the momentum balance we predict the scaled partitioning

$$\frac{\overline{\Delta\langle n\rangle}}{n^\infty} = \frac{\int_0^{d/2}\left[1 - \frac{\Pi^W(y)}{\Pi^\infty}\right]dy}{\int_0^\Delta\left[1 - \frac{\Pi^W(y)}{\Pi^\infty}\right]dy}. \qquad (18)$$

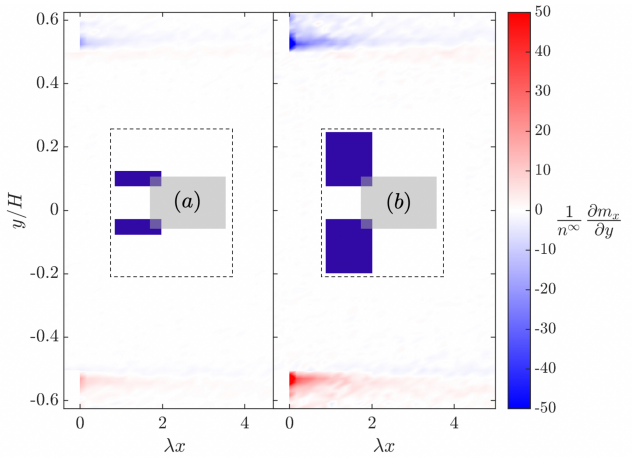

Fig. 10 The change in polar order distribution in the y-direction, $(\mathrm{d}m_x/\mathrm{d}y)/n^\infty$, around the opening for (a) the parallel plates and (b) the channel geometry for $\ell/H = 3$ and $k_sT_s/k_BT \sim 3 \cdot 10^2$. The gray regions illustrate the area for which the change in polar order is shown.

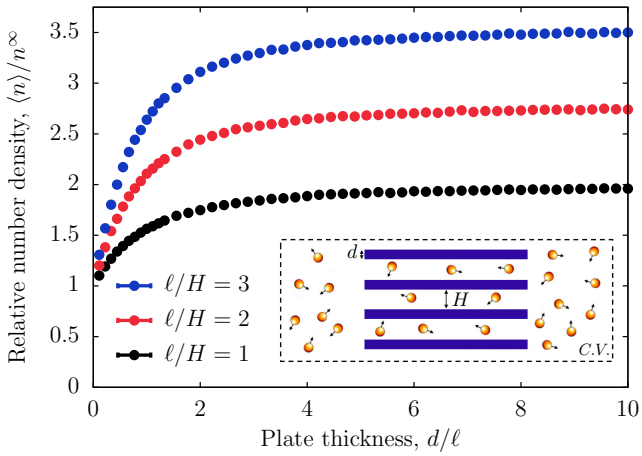

Fig. 11 Normalized number density in the channels as a function of plate thickness for $k_sT_s/k_BT = 1012.5$ and $L/\ell = 10$. The inset shows the illustration of periodic plates, where d is the plate thickness and H is the separation between the plates.

And by assuming that the decrease in concentration (and thus pressure) near the corners has exactly the same functional form independent of the plate thickness, we can use the data for wall pressure obtained for the single channel. We applied the Π^W determined from BD simulations with $k_sT_s/k_BT = 128$, $L/H = 7.5$, and $\ell/H = 2$ in (4), and Fig. 12 shows excellent agreement between the prediction and the periodic plates simulations. This shows that the wall pressure follows the same functional form at the corners independent of plate thickness. Further, we see that the number density plateaus at a plate thickness of $d/\ell \approx 6$, which corresponds to twice the deficit distance. This is the smallest thickness needed to obtain the full concentration deficit near the plate corners and thereby obtain the maximum concentration between the plates. Adding additional thickness to the plates will have no effect on the partitioning between the channels and the reservoir.

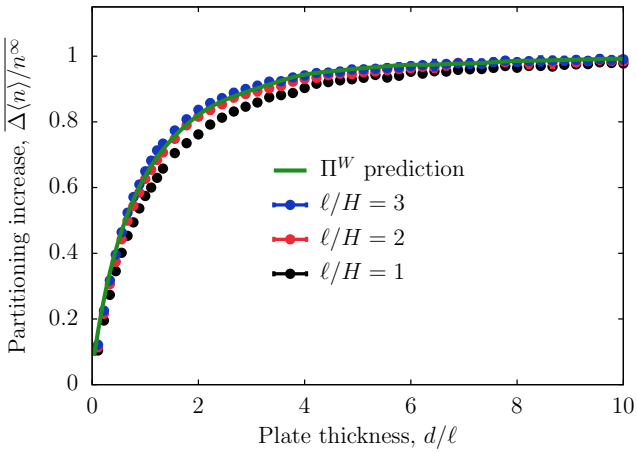

Fig. 12 Partitioning increase as a function of the plate thickness (see equation (17)) both for Brownian Dynamics simulation and that predicted from the momentum balance.

5 Conclusions

The attraction (Casimir effect) between parallel plates in a bath of active particles increases with increasing degree of particle confinement (run length per plate spacing). Through a simple macroscopic mechanical momentum balance we presented a method to predict the attraction that agrees well with BD simulations and solution of the full Smoluchowski equation. The prediction has no adjustable parameters. This method was extended to the partitioning of ABPs between a channel and an infinite reservoir. In contrast to the parallel plates where the average concentration between the plates is the same as in the reservoir for all degrees of confinement, for the channel the average concentration in the channel grows linearly with the degree of confinement. It was shown that this results from a deficit of ABPs on walls of the reservoir near the channel opening. It is important to appreciate that the different behaviors in the two geometries results from the inherent nonequilibrium nature of the active particle dynamics; an equilibrium system would show no difference in the two geometries.

We hope that this simple approach of macroscopic momentum balances can be extended to other confinement problems and allow one to understand and predict behavior without having to perform computationally costly finite element calculations or Brownian Dynamics simulations. Additionally, utilizing the insights in partitioning behavior for these fundamental geometries will be valuable in designing optimal structures for enhancing or isolating active particles.

A Brownian Dynamics simulations

The equations of motion implemented are the overdamped Langevin equations[24]:

$$\mathbf{0} = -\zeta \boldsymbol{u}_\alpha + \boldsymbol{F}_\alpha^{Swim} + \boldsymbol{F}_\alpha^B + \boldsymbol{F}_\alpha^W, \tag{19}$$

$$\mathbf{0} = -\zeta_R \boldsymbol{\Omega}_\alpha + \boldsymbol{L}_\alpha^R, \tag{20}$$

where $\boldsymbol{U}_\alpha$ is the translational velocity, $\boldsymbol{\Omega}_\alpha$ is the rotational velocity, ζ_R is the rotational Stokes drag coefficient, and $\boldsymbol{F}_\alpha^{Swim}$ is the swim force defined as $\boldsymbol{F}_\alpha^{Swim} \equiv \zeta U_0 \boldsymbol{q}_\alpha$. $\boldsymbol{F}_\alpha^B$ is the random Brownian force with the properties $\overline{\boldsymbol{F}_\alpha^B} = \mathbf{0}$ and the $\overline{\boldsymbol{F}_\alpha^B(0)\boldsymbol{F}_\alpha^B(t)} = 2k_BT\zeta\delta(t)\boldsymbol{I}$, where $\boldsymbol{I}$ is the identity tensor and $\delta(t)$ is the delta-function. $\boldsymbol{L}^R$ is the random reorientation torque, where $\overline{\boldsymbol{L}^R} = \mathbf{0}$ and $\overline{\boldsymbol{L}^R(0)\boldsymbol{L}^R(t)} = 2\zeta_R^2\delta(t)\boldsymbol{I}/\tau_R$. The simulations length scale is non-dimensionalized by the microscopic length $\delta = \sqrt{D_T/D_R}$ and the time steps are non-dimensionalized by the reorientation time τ_R, where $\tau_R = 1/D_R$ and $D_T = k_BT/\zeta$. Note that it is not necessary to assume that the translational and rotational diffusivities are both thermal, i.e. D_R need not be proportional to k_BT. Changes in orientation follow from $d\boldsymbol{q}/dt = \boldsymbol{\Omega} \times \boldsymbol{q}$, with $\boldsymbol{\Omega}$ from the particle angular momentum balance (20).

The particles are ideal and therefore only interact with the walls (no-flux boundaries) through the potential-free algorithm that models a hard-particle force.[26–28] This algorithm is implemented by placing a particle that overlaps with a wall back to the point of contact following along the boundaries normal vector until the system is free of overlaps.

We can determine the wall pressure from measuring the force on the wall per area, $\boldsymbol{F}^W/A$. The force exerted by an ABP on the wall is determined by measuring displacements at the wall. The force one ABP α exerts is

$$\boldsymbol{F}_\alpha^W = \zeta U_\alpha^{overlap} \boldsymbol{n} = \zeta \frac{\Delta x^{overlap}}{\Delta t} \boldsymbol{n}, \tag{21}$$

where $\Delta x^{overlap}$ is the overlap measured normal to the wall before the collision is resolved and Δt is the size of the time step. From the force exerted by the individual particles the pressure at position z is given by

$$\Pi^W(z) = \sum_i^N \frac{\zeta U_i^{overlap}}{\Delta z}. \tag{22}$$

Conflicts of interest

There are no conflicts to declare.

Acknowledgements

The authors would like to thank S. Takatori, A. Dulaney and T. Zhou for insightful discussions. This work was supported in part by the National Science Foundation under Grant No. 1803662.

References

1 E. Lauga and T. R. Powers, Reports on Progress in Physics, 2009, **72**, 096601.
2 S. Granick, S. Jiang and Q. Chen, Physics Today, 2009, **62**, 68–69.
3 F. Wurm and A. F. M. Kilbinger, Angewandte Chemie-international Edition, 2009, **48**, 8412–8421.
4 S. C. Takatori and J. F. Brady, Current Opinion in Colloid and Interface Science, 2016, **21**, 24–33.
5 S. Ramaswamy, Annual Review of Condensed Matter Physics, 2010, **1**, 323–345.
6 S. A. Mallory, C. Valeriani and A. Cacciuto, Annual Review of Physical Chemistry, 2018, **69**, 59–79.
7 C. Maggi, J. Simmchen, F. Saglimbeni, J. Katuri, M. Dipalo, F. De Angelis, S. Sanchez and R. Di Leonardo, Small, 2016, **12**, 446–451.
8 C. Bechinger, R. Di Leonardo, H. Löwen, C. Reichhardt, G. Volpe and G. Volpe, Rev. Mod. Phys., 2016, **88**, 045006.
9 D. A. Beard and T. Schlick, Biophysical Journal, 2003, **85**, 2973–2976.
10 S. C. Takatori, R. De Dier, J. Vermant and J. F. Brady, Nature Communications, 2016, **7**, 10694.
11 W. M. Lai, D. Rubin and E. Krempl, Introduction to continuum mechanics, revised edition, Pergamon, 1978, p. 324.
12 B. Ezhilan, R. Alonso-Matilla and D. Saintillan, Journal of Fluid Mechanics, 2015, **781**, R4.
13 W. Yan and J. F. Brady, Journal of Fluid Mechanics, 2015, **785**, R1.
14 X. Yang, L. Manning and C. Marchetti, Soft Matter, 2014, **10**, 6477–6484.
15 P. Galajda, J. Keymer, P. Chaikin and R. Austin, Journal of Bacteriology, 2007, **189**, 8704–8707.
16 R. Di Giacomo, S. Krödel, B. Maresca, P. Benzoni, R. Rusconi, R. Stocker and C. Daraio, Scientific Reports, 2017, **7**, 1–8.
17 D. Ray, C. Reichhardt and C. J. O. Reichhardt, Physical Review E, 2014, **90**, 013019.
18 B. V. Derjaguin, Y. I. Rabinovich and N. V. Churaev, Nature, 1978, **272**, 313–318.
19 T. Franosch, S. Lang and R. Schilling, Physical Review Letters, 2012, **109**, 1–5.
20 G. Bressi, G. Carugno, R. Onofrio, G. Ruoso, R. Onofrio and G. Ruoso, Physical Review Letters, 2002, **88**, 4.
21 S. K. Lamoreaux, Reports on Progress in Physics, 2005, **68**, 201–236.
22 P. Jenkins and M. Snowden, Advances in Colloid and Interface Science, 1996, **68**, 57–96.
23 R. A. Robinson and R. H. Stokes, Electrolyte solutions: the measurement and interpretation of conductance, chemical potential, and diffusion in solutions of simple electrolytes, Academic Press, 1959, p. 76.
24 W. Yan and J. F. Brady, Soft Matter, 2015, **11**, 6235–6244.
25 S. C. Takatori, W. Yan and J. F. Brady, Physical Review Letters, 2014, **113**, 1–5.
26 D. M. Heyes and J. R. Melrose, Journal of Non-Newtonian Fluid Mechanics, 1993, **46**, 1–28.
27 W. Schaertl and H. Sillescu, Journal of Statistical Physics, 1994, **74**, 687–703.

28 D. R. Foss and J. F. Brady, Journal of Rheology, 2000, **44**, 629–651.
29 F. Hecht, J. Numer. Math., 2012, **20**, 251–265.

A theoretical model based on macroscopic momentum balances analytically predicts the Casimir effect and the partitioning of active matter.